

AARHUS UNIVERSITY

DEPARTMENT OF MECHANICAL AND PRODUCTION
ENGINEERING

DYNAMIC SYSTEMS WITH APPLICATION - GROUP 9

Dynamics of an Elevator with Elastic Ropes

Student:

Frederik Fristed
Katharina Brarup Schäfer
Petar Gavran
Rune Marsilius Jensen
Thea Gorzelak

Student number:

201805718
201710730
202102200
201808110
201807917



AARHUS UNIVERSITY

April 20 2022

Contents

1	Dynamics of an elevator with elastic ropes	1
1.1	Modeling the elevator as a discrete system	1
1.2	Identification of all the parameters	3
1.3	Experimental test	4
1.4	Numerical simulation of the elevator dynamics	7
1.5	Validation of simulation results	8
1.6	Conclusion	11
A	Rope experiment	12

1 | Dynamics of an elevator with elastic ropes

The purpose of this project is to investigate the dynamics of an elevator-system modeled with elastic ropes. The report will go through the simulation of the elevator-system as a discrete system. The results from the numerical simulation are then compared and validated using virtual experiment data from an imagined elevator ride where the cabin moves upwards. Originally, it was within the scope of this project to perform an experiment on a physical elevator-system to determine relevant parameters, such as the effective radius of the drive sheave, and to validate the numerical simulation. However, because the test setup malfunctioned, it has not been possible to perform the experiment.

1.1 Modeling the elevator as a discrete system

The elevator-system modeled with elastic ropes is shown in Fig. 1.1. The global coordinate system is defined from the ground, where the Y-axis is parallel to the ground and the Z-axis is perpendicular to the ground with a positive direction upwards. The elastic ropes are modeled as an equivalent spring-damper mass system, as illustrated in Fig. 1.1. Note that in this project, the mass of the rope is not included in the equations of motion. The implications of this simplification are discussed in Section 1.5.

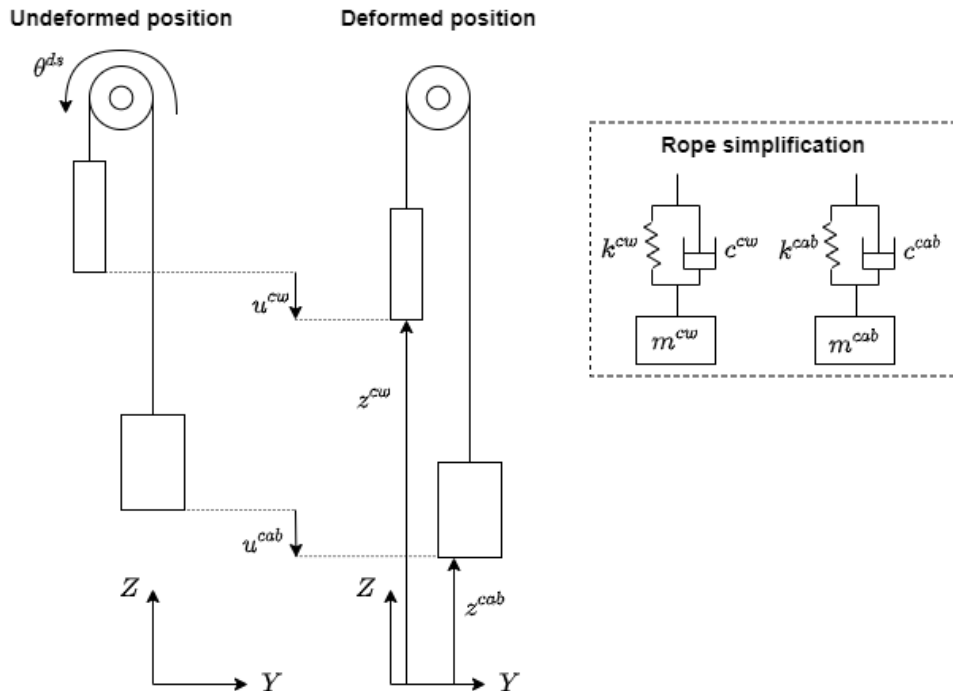


Figure 1.1: System drawing of the elevator with elastic ropes

Assumptions

The numerical simulation of the elevator-system is based on the following assumptions:

- Drive sheave and drive sheave support are rigid.
- There is no slip between the rope and the drive sheave. The arc length covered by the drive sheave's angular rotation is equal to the translation of the rope.
- The rope can be considered as two separate rope segments divided by the point of no-slip.
- The rope has no mass. The rope is shaped like a rod and behaves like a spring.
- The damping coefficient of the rope is linearly proportional to the stiffness of the rope.

Derivation of the equations of motion for the elevator-system

The equation of motion (EOM) for the system is obtained using Lagrange's equations of motion, as stated in Eq. (1.1).

$$\frac{d}{dt} \left(\frac{\partial L}{\partial \dot{q}} \right) - \frac{\partial L}{\partial q} + \frac{\partial F}{\partial \dot{q}} = Q_{app} \quad (1.1)$$

Where the Lagrangian, L , is defined as the kinetic energy minus the potential energy: $L = T - U$ and the generalised coordinates are: $\mathbf{q} = [\theta^{ds} \ u^{cab} \ u^{cw}]^T$. The kinetic energy consists of the kinetic energy for the drive sheave, cabin and counterweight.

$$T = \frac{1}{2} \cdot I_{eq}^{ds} \cdot (\dot{\theta}^{ds})^2 + \frac{1}{2} \cdot m^{cab} \cdot (R\dot{\theta}^{ds} - \dot{u}^{cab})^2 + \frac{1}{2} \cdot m^{cw} \cdot (-R\dot{\theta}^{ds} - \dot{u}^{cw})^2 \quad (1.2)$$

The potential energy consists of the gravitational energy for the cabin and counterweight and deformation energy for the ropes.

$$U = m^{cab}g(z_0^{cab} + \theta^{ds}R - u^{cab}) + m^{cw}g(z_0^{cw} - \theta^{ds}R - u^{cw}) + \frac{1}{2} \frac{EA}{l^{cab}} u^{cab^2} + \frac{1}{2} \frac{EA}{l^{cw}} u^{cw^2} \quad (1.3)$$

The internal damping of the rope is taken into account through Rayleigh's dissipation function, F . The dissipation function expresses the linear velocity-dependent dissipative forces in the rope. Writing the equation out in terms of the cabin and the counterweight, the following expression is obtained.

$$F = \frac{1}{2} \cdot c^{cab} \cdot (\dot{u}^{cab})^2 + \frac{1}{2} \cdot c^{cw} \cdot (\dot{u}^{cw})^2 \quad (1.4)$$

The generalized applied forces of the system are equal to the applied motor torque from the drive sheave. The motor torque is only imposed on the generalized coordinate θ^{ds} .

$$\mathbf{Q}_{app} = [M^{ds} \ 0 \ 0]^T$$

Inserting the kinetic and potential energies, Rayleigh's dissipation function, and the generalized applied force in Eq. (1.1) and determining the derivatives yields three equations. By rearranging them it is possible to express the equation of motion in state space formulation.

$$\mathbf{M} \cdot \ddot{\mathbf{q}} + \mathbf{C} \cdot \dot{\mathbf{q}} + \mathbf{K} \cdot \mathbf{q} = \mathbf{Q}_{grav} + \mathbf{Q}_{elastic} \quad (1.5)$$

Where the above entities are as follows.

$$\mathbf{M} = \begin{bmatrix} I_{eq}^{ds} + (m^{cw} + m^{cab}) \cdot R^2 & -m^{cab} \cdot R & m^{cw} \cdot R \\ -m^{cab} \cdot R & m^{cab} & 0 \\ m^{cw} \cdot R & 0 & m^{cw} \end{bmatrix}$$

$$\mathbf{C} = \begin{bmatrix} 0 & 0 & 0 \\ 0 & c^{cab} & 0 \\ 0 & 0 & c^{cw} \end{bmatrix} \quad \mathbf{K} = \begin{bmatrix} 0 & 0 & 0 \\ 0 & \frac{E \cdot A}{l^{cab}} & 0 \\ 0 & 0 & \frac{E \cdot A}{l^{cw}} \end{bmatrix} \quad \mathbf{Q}_{elastic} = \begin{bmatrix} M^{ds} \\ 0 \\ 0 \end{bmatrix} \quad \mathbf{Q}_{grav} = \begin{bmatrix} (m^{cw} - m^{cab}) \cdot g \cdot R \\ m^{cab} \cdot g \\ m^{cw} \cdot g \end{bmatrix}$$

For simplicity and convenience, the generalised coordinates are divided into two sets: the coordinates concerning rotational motion and the coordinates concerning the translational motion, as follows:

$$\mathbf{q} = \begin{bmatrix} \mathbf{q}_1 \\ \mathbf{q}_2 \end{bmatrix} \quad \mathbf{q}_1 = \begin{bmatrix} \theta^{ds} \end{bmatrix} \quad \mathbf{q}_2 = \begin{bmatrix} u^{cab} \\ u^{cw} \end{bmatrix}$$

Using the division of generalised coordinates, the EOM can be rewritten as:

$$\begin{bmatrix} \mathbf{M}_{11} & \mathbf{M}_{12} \\ \mathbf{M}_{21} & \mathbf{M}_{22} \end{bmatrix} \cdot \begin{bmatrix} \ddot{\mathbf{q}}_1 \\ \ddot{\mathbf{q}}_2 \end{bmatrix} + \begin{bmatrix} \mathbf{C}_{11} & \mathbf{C}_{12} \\ \mathbf{C}_{21} & \mathbf{C}_{22} \end{bmatrix} \cdot \begin{bmatrix} \dot{\mathbf{q}}_1 \\ \dot{\mathbf{q}}_2 \end{bmatrix} + \begin{bmatrix} \mathbf{K}_{11} & \mathbf{K}_{12} \\ \mathbf{K}_{21} & \mathbf{K}_{22} \end{bmatrix} \cdot \begin{bmatrix} \mathbf{q}_1 \\ \mathbf{q}_2 \end{bmatrix} = \begin{bmatrix} \mathbf{Q}_{grav1} \\ \mathbf{Q}_{grav2} \end{bmatrix} + \begin{bmatrix} \mathbf{Q}_{elastic1} \\ \mathbf{Q}_{elastic2} \end{bmatrix} \quad (1.6)$$

1.2 Identification of all the parameters

The parameters used for defining the model of the elevator as a discrete system will be explained in this section.

The coordinates used to define the system are: $\theta^{ds}, z^{cab}, z^{cw}, u^{cab}, u^{cw}$.

The positions of the cabin and counterweight are defined as:

$$\begin{aligned} z^{cab} &= z_0^{cab} + \theta^{ds} R - u^{cab} \\ z^{cw} &= z_0^{cw} - \theta^{ds} R - u^{cw} \end{aligned}$$

The initial position of the cabin, z_0^{cab} , is taken from virtual data at time $t = 0$. The initial position of the counterweight, z_0^{cw} , can be calculated from the position of the cabin.

According to the diagram in Fig. 1.1 of the 3 DoF elevator system with flexible ropes and given initial data from the virtual experiment, the calculation for initial positions in static equilibrium can be performed, as shown in Eq. (1.8) and Eq. (1.10). With the known total length of the rope, l^{total} , and the elongated length of rope on the cabin side, l^{cab} , which is provided in the virtual experiment data, the rest of the initial calculation parameters can be done.

The undeformed length of the rope on the cabin side can be calculated as follows, where the relation used can be derived from force balance:

$$l_0^{cab} = \frac{l^{cab}}{1 + \frac{m^{cab} \cdot g}{EA}} \quad (1.7)$$

From this, the deformation of the rope on the cabin side can be expressed as:

$$u_0^{cab} = \frac{m^{cab} \cdot g \cdot l_0^{cab}}{EA} \quad (1.8)$$

Following the same procedure, as shown above, the undeformed length of the rope on the counterweight side and deformation of the rope on the counterweight side can be expressed as:

$$l_0^{cw} = \frac{l^{cw}}{1 + \frac{m^{cw} \cdot g}{EA}} \quad (1.9)$$

$$u_0^{cw} = \frac{m^{cw} \cdot g \cdot l_0^{cw}}{EA} \quad (1.10)$$

Individual parameters that were used to define the model of the elevator as a discrete system are the mass of the cabin (m^{cab}), the mass of the counterweight (m^{cw}), the initial position of the cabin (z_0^{cab}), the initial position of the counterweight (z_0^{cw}), the total moment of inertia of the system (I_{eq}^{ds}), the drive sheave radius (R) and the angular rotation of the drive sheave (θ^{ds}).

The angular rotation of the drive sheave, θ^{ds} , is read from the virtual experiment data. Here, an encoder with 3200 pulses/rev is installed on the shaft of the motor, where it measures rotation in pulses. Encoder pulses N_p^{ds} are translated into angular rotations as:

$$\theta^{ds} = \frac{N_p^{ds}}{N} \cdot \frac{2\pi}{3200} \quad (1.11)$$

Where N is the gearbox ratio from the virtual experiment, found in Table 1.1.

1.3 Experimental test

For this project, an experiment on the elevator ride was supposed to be carried out, which should provide parameters and data in order to make a verification of the numerical simulation and some measured data. By determining the effective drive sheave radius, the simulation should be refined. Unfortunately, the experiment did not work, so no data was collected. However, it was possible to conduct an experiment with a piece of rope to determine the ropes stiffness and internal viscous damping, which can be read in Appendix A.

In order to perform a validation of the numerical simulation, some virtual experimental data was given and is used for this. Because the virtual experiment has nothing to do with the actual experiment of the elevator ride, the experimental rope parameters presented in Appendix A cannot be used.

In the following, the virtual experimental data is presented, and the supposed elevator experiment is described. To perform both the rope experiment and the supposed elevator experiment, an accelerometer is used and is calibrated according to the description at the end of this section.

Virtual experiment

Because the elevator experiment is not working, there will be used values from a virtual experiment instead of test values from the elevator experiment. This gives simulated values for a system equivalent to the one shown on Fig. 1.2. Table 1.1 shows the given variables from the virtual experiment.

Description	Symbol	Value
Mass of the cabin	m^{cab}	0.5 kg
Mass of the counterweight	m^{cw}	0.6 kg
Mass of the gear motor	m^{mot}	1.942 kg
Moment of inertia of drive sheave	I^{ds}	$4 \times 10^{-5} \text{ kg} \cdot \text{m}^2$
Moment of inertia of rotor of motor	I^{mot}	$5 \times 10^{-6} \text{ kg} \cdot \text{m}^2$
Rope total length	L	2.75 m
Rope stiffness per unit length	EA	85 N
Drive sheave radius	R	49 mm
Gear ratio of gear box	N	1/160
Length of rope on cabin side	l^{cab}	2106 mm
Encoder parameter	—	3200 pulses/rev
Gravity	g	9.81 m/s ²

Table 1.1: System parameters and conditions of the experiment

The rope's viscous damping coefficient, which is individual for the cabin and counterweight side of the rope:

$$c = 0.001 \frac{\frac{N \cdot s}{m}}{\frac{N}{m}} \cdot \frac{EA}{l} \quad (1.12)$$

Test results from the virtual experiment consist of a matrix with four columns of data. The data given is the time, the encoder pulses, the distance from the bottom of the tube to the bottom of the cabin, and the acceleration of the cabin.

Filtering

The virtual experimental data regarding the cabin position and cabin acceleration contains noise, which needs to be removed. This is done by applying a Butterworth low-pass filter to the signals and thereby generating a signal without noise. The cut-off frequency used to perform the low-pass filtering is determined by plotting the unfiltered data in the frequency domain and from that reading an appropriate cut-off frequency. Both the filtered and unfiltered data are shown in Fig. 1.4 the following Section 1.5.

Elevator Experiment

The purpose of the elevator experiment is to measure the cabin height, cabin acceleration, and angle rotation of the drive sheave for a small-scale elevator setup. To collect data from the experiment, the following relevant sensors are needed: an ultrasonic distance sensor to collect the cabin height, an accelerometer to collect the cabin acceleration, an encoder to collect the angular rotation of the drive sheave, and an Arduino or some other board for interacting with the sensors and the computer.

Experimental setup

The test setup consists of an elevator tube frame of 4 tubes, and in the middle, there are two PVC tubes. Inside the PVC tubes are a cabin and a counterweight. The cabin and the counterweight are connected with a flexible rope, which is driven by an electric motor. Beneath the cabin, on the floor, is an ultrasonic distance sensor to measure the height of the cabin. On the cabin, an accelerometer is mounted, and on the motor, an encoder is mounted.

1.3. EXPERIMENTAL TEST

From the encoder pulses, a drive sheave position can be obtained.

In short, the experiment is simply moving the elevator cabin from the bottom to the top of the tube while collecting data. The test setup is illustrated in Fig. 1.2.

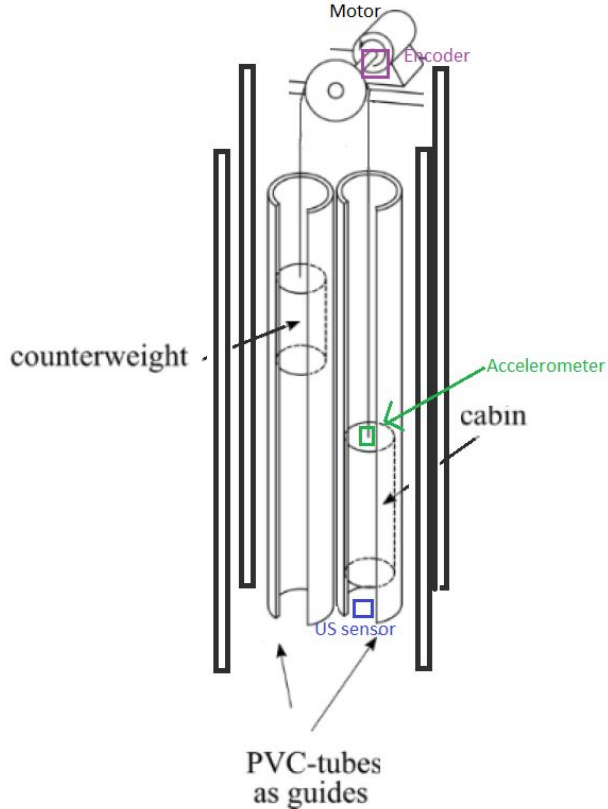


Figure 1.2: System drawing of the test setup

Calibration of accelerometer

The stiffness and damping of the rope are determined in appendix A. Before doing these experiments, the accelerometer must be calibrated. Accelerometers do not show the exact acceleration, so to be able to get numbers closer to the real acceleration, calibration needs to be performed. The relationship between the normalized A_{x1} , A_{y1} and A_{z1} and the accelerometer raw measurements A_x , A_y and A_z can be expressed as:

$$\begin{bmatrix} A_{x1} \\ A_{y1} \\ A_{z1} \end{bmatrix} = [A_m]_{3x3} \begin{bmatrix} \frac{1}{A_{SCx}} & 0 & 0 \\ 0 & \frac{1}{A_{SCy}} & 0 \\ 0 & 0 & \frac{1}{A_{SCz}} \end{bmatrix} \cdot \begin{bmatrix} A_x - A_{OSx} \\ A_y - A_{OSy} \\ A_z - A_{OSz} \end{bmatrix} \quad (1.13)$$

$$= \begin{bmatrix} ACC_{11} & ACC_{12} & ACC_{13} \\ ACC_{21} & ACC_{22} & ACC_{23} \\ ACC_{31} & ACC_{32} & ACC_{33} \end{bmatrix} \cdot \begin{bmatrix} A_x \\ A_y \\ A_z \end{bmatrix} + \begin{bmatrix} ACC_{10} \\ ACC_{20} \\ ACC_{30} \end{bmatrix}$$

Where A_m is the 3x3 misalignment matrix between the accelerometer sensing axes and the device body axes, A_{SCi} ($i = x, y, z$) is the sensitivity (or scale factor) and A_{OSi} is the zero-g level (or offset). The goal of the accelerometer calibration is to determine 12 parameters from ACC_{10} to ACC_{33} , so that with any given raw measurements at arbitrary positions, the normalized values A_{x1} , A_{y1} and A_{z1} can be obtained.

The calibration is performed by measuring 6 stationary positions, at 10 seconds each. Each

measurement gives the gravity at that specific orientation. The equation to determine the calibration matrix can be written as:

$$Y = W \cdot X \quad (1.14)$$

Where X is the calibration matrix, W is the raw sensor data collected from the 6 stationary measurements and Y is the normalized gravity vector, written in the same order as the measurements are performed.

The calibration matrix can be determined with the least square method:

$$X = (W^T \cdot W)^{-1} \cdot W^T \cdot Y \quad (1.15)$$

1.4 Numerical simulation of the elevator dynamics

To describe and visualize the mathematical model that is used to simulate the elevator dynamics, a flowchart of the code is created, which can be seen in Fig. 1.3. The numerical simulation uses the angular rotation of the drive sheave, θ^{ds} , as the driving variable. The angular rotation is read from the virtual experiment data. In this way, only part of the EOM needs to be solved, and \dot{u}^{cab} and \ddot{u}^{cw} can be obtained without knowing the motor torque on the drive sheave, M^{ds} , which is unknown at this stage.

$$\mathbf{M}_{22}\ddot{\mathbf{q}}_2 = \mathbf{Q}_{grav2} + \mathbf{Q}_{elastic2} - \mathbf{M}_{21}\dot{\mathbf{q}}_1 - \mathbf{C}_{21}\dot{\mathbf{q}}_1 - \mathbf{C}_{22}\dot{\mathbf{q}}_2 - \mathbf{K}_{21}\mathbf{q}_1 - \mathbf{K}_{22}\mathbf{q}_2 \quad (1.16)$$

The compact division form of the EOM from Eq. (1.16) is solved by taking the inverse of \mathbf{M}_{22} and using MatLab's integrated Runge-Kutta ODE solver , ODE45, by giving it the initial conditions for \mathbf{y} and $\dot{\mathbf{y}}$ and solving for each time step by stepping through time. Here, \mathbf{y} is defined as:

$$\mathbf{y} = \begin{bmatrix} \mathbf{q} \\ \dot{\mathbf{q}} \end{bmatrix} = \begin{bmatrix} \theta^{ds} & u^{cab} & u^{cw} & \dot{\theta}^{ds} & \dot{u}^{cab} & \dot{u}^{cw} \end{bmatrix}^T$$

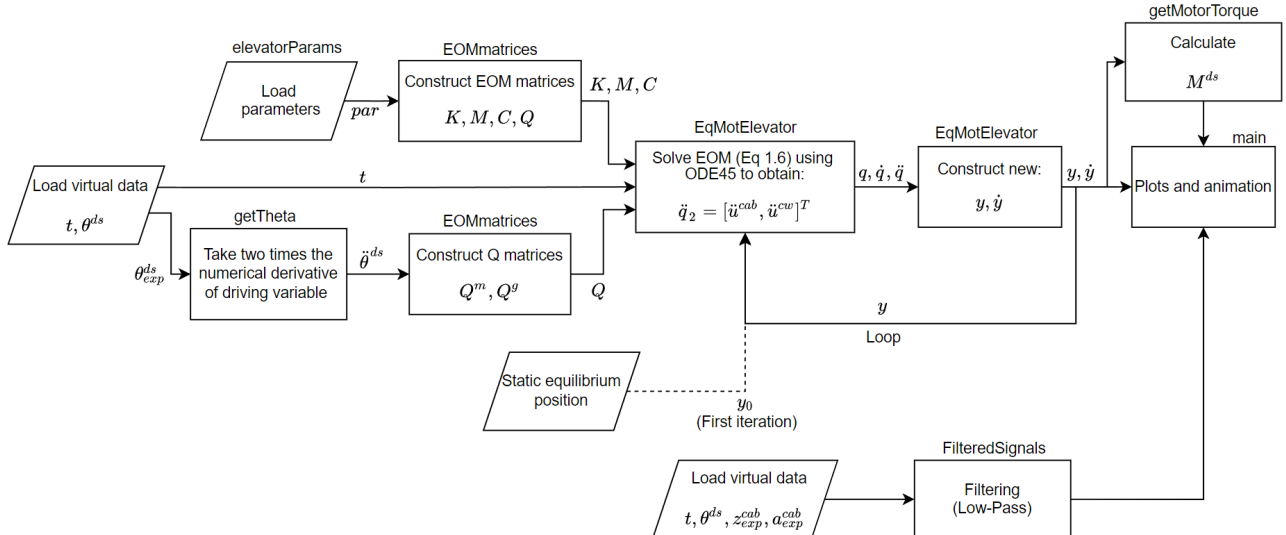


Figure 1.3: Flowchart showing how the mathematical model is executed

The drive sheave angle, θ^{ds} , is numerically differentiated twice using spline functions to obtain the angular velocity, $\dot{\theta}^{ds}$, and the angular acceleration, $\ddot{\theta}^{ds}$. When $\dot{\theta}^{ds}$ is known and the EOM

is solved, the motor torque can be calculated directly from Eq. (1.17), which accounts for the contribution to the torque from the tension in the rope on both cabin and counterweight side.

$$M^{ds} = I_{eq}^{ds} \cdot \ddot{\theta}^{ds} + m^{cab} \cdot R \cdot (g + R\ddot{\theta}^{ds} - \ddot{u}^{cab}) - m^{cw} \cdot R \cdot (g + R\ddot{\theta}^{ds} - \ddot{u}^{cw}) + M^{brake} \quad (1.17)$$

In Eq. (1.17), the moment that the brake has to deliver is determined as the accelerating mass that has to be stopped.

$$M^{brake} = (m_{\text{cabin}} + m_{\text{counterweight}}) \cdot g \cdot R$$

The total equivalent moment of inertia, I_{eq}^{ds} , consists of the moment of inertia of the drive sheave, the rotor of the motor, and the contribution from the cabin and counterweight masses. However, the gear reduces the load inertia reflected to the motor. It is necessary to take the reflected inertia into account. This is done by dividing with the gear ratio squared in the term containing the moment of inertia of the rotor of the motor.

$$I_{eq}^{ds} = I^{ds} + \frac{I^{mot}}{N^2} + (m^{cab} + m^{cw}) \cdot R^2 \quad (1.18)$$

The results of the numerical simulation are presented in the following Section 1.5.

1.5 Validation of simulation results

To perform a validation of the simulation results, the simulated cabin position and acceleration are compared to the virtual experiment data. The position and acceleration is shown in Fig. 1.4 in the time domain and in Fig. 1.5 in the frequency domain. Fig. 1.4 shows that the simulated position of the cabin is very similar to the position obtained using the filtered virtual data. Looking at the accelerations it can be read that the shape of the simulated cabin acceleration is relatively in agreement with the virtual data, however, the amplitudes are displaced relative to each other, indicating that a phase shift has been introduced in the simulation. This phase shift is a result of the numerical differentiation that is performed twice to obtain the angular acceleration of the drive sheave, which is used to determine the simulated cabin acceleration.

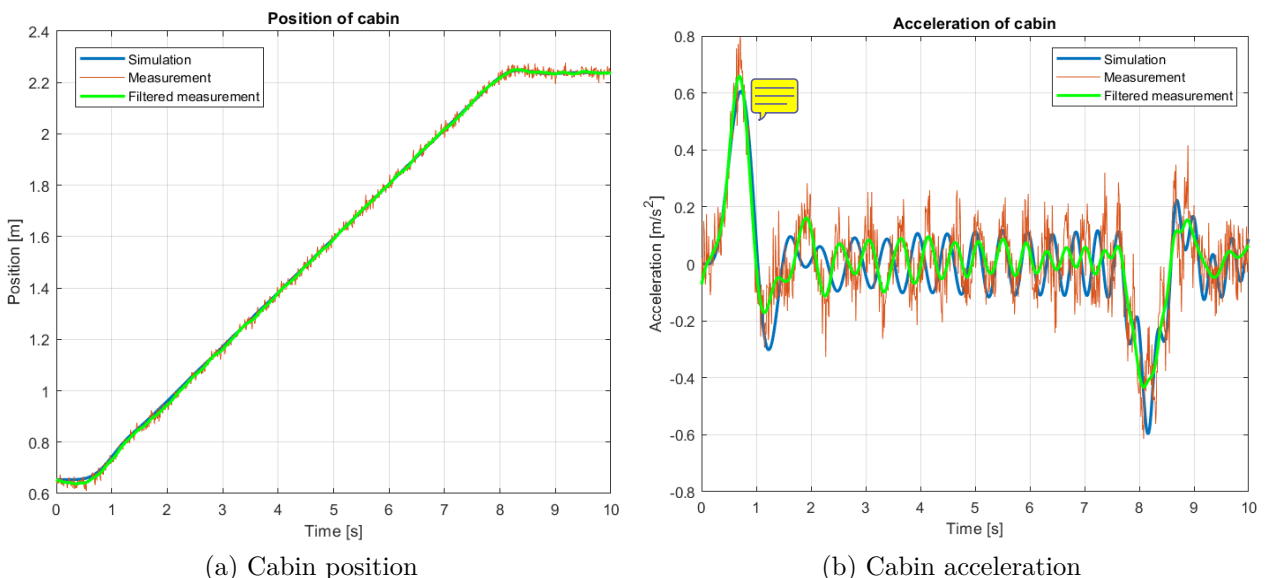


Figure 1.4: Cabin position and acceleration in time domain for the simulated data and filtered and unfiltered virtual data.

1.5. VALIDATION OF SIMULATION RESULTS

From Fig. 1.5, which shows the results in the frequency domain, it can be read that the simulated results and filtered virtual data have the same dominant frequencies because the amplitude spikes have similar heights and appear at the same frequencies, which verifies the simulated results despite the introduced phase shift. Especially, the plot of the cabin position in the frequency domain shows an exact agreement between the results, and thereby again validates the simulated position of the cabin.

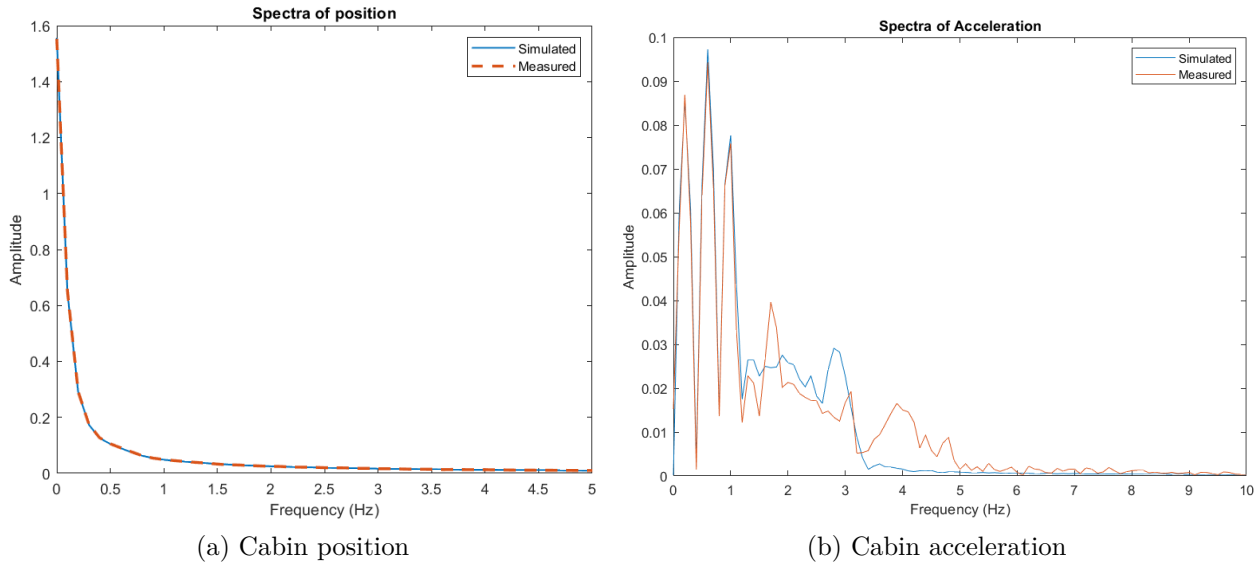


Figure 1.5: Cabin position and acceleration in frequency domain for the simulated data and the filtered virtual data.

As a part of the exercise, the tension of the rope on the cabin side was determined, which is plotted for both the simulated results and the virtual data as shown in Fig. 1.6. The tensile force is determined from force equilibrium by assuming a no-slip condition at the drive sheave, thus only having the contribution of forces from gravity and the accelerating mass. As stated earlier in the report, the mass of the ropes is not included in this model of the elevator, where the flexible ropes are simplified to mass-less springs and dampers. The effect of not including the mass of the ropes can be seen from the tensile force because it varies around a constant value in the period where a constant velocity is obtained. If the mass of the rope was included, it would not vary around a constant value, but instead, have a decreasing slope on the cabin side (and an increasing slope on the counterweight side).

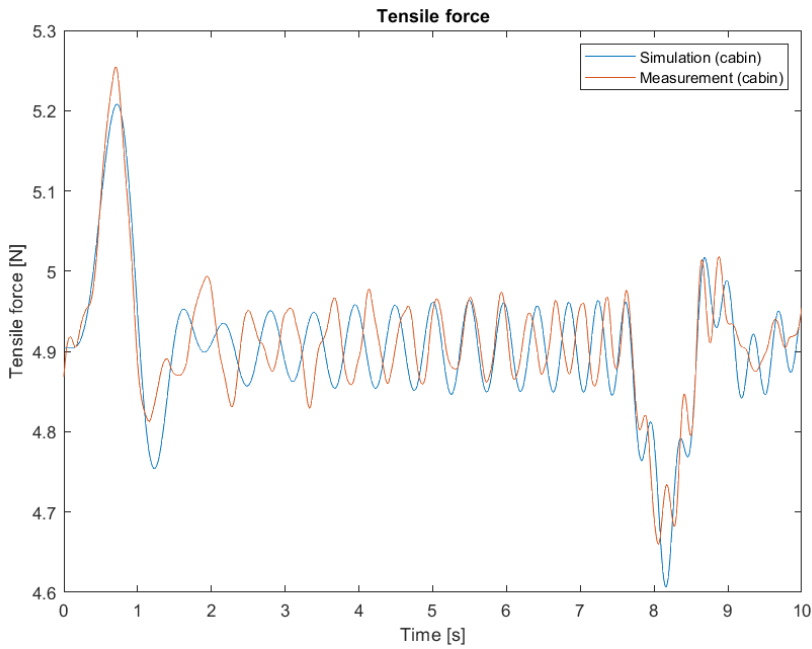


Figure 1.6: Tensile force in rope on the cabin side for the simulated and the filtered virtual data

Fig. 1.7 shows the velocity of the cabin in the time domain. Here, the simulated velocity is compared to the virtual experiment data. In the virtual experiment, the velocity of the cabin is not measured directly. However, this experimental velocity can be obtained by two methods. First, by taking the numerical derivative of the measured cabin position. This derivative is taken using the central differences method. The numerical derivative is shown in Fig. 1.7. Note, that this derivative has been filtered a second time because numerical differentiation amplifies noise. The second method is by numerical integration of the measured cabin acceleration. This is also shown in Fig. 1.7. The figure shows that both of these numerical methods yield velocities similar to the simulation. The numerical integration has clearly introduced a linear drift to the results, increasing with time, which is normal for this method. Because the initial and final velocities are known, a correction can be made to remove this drift.

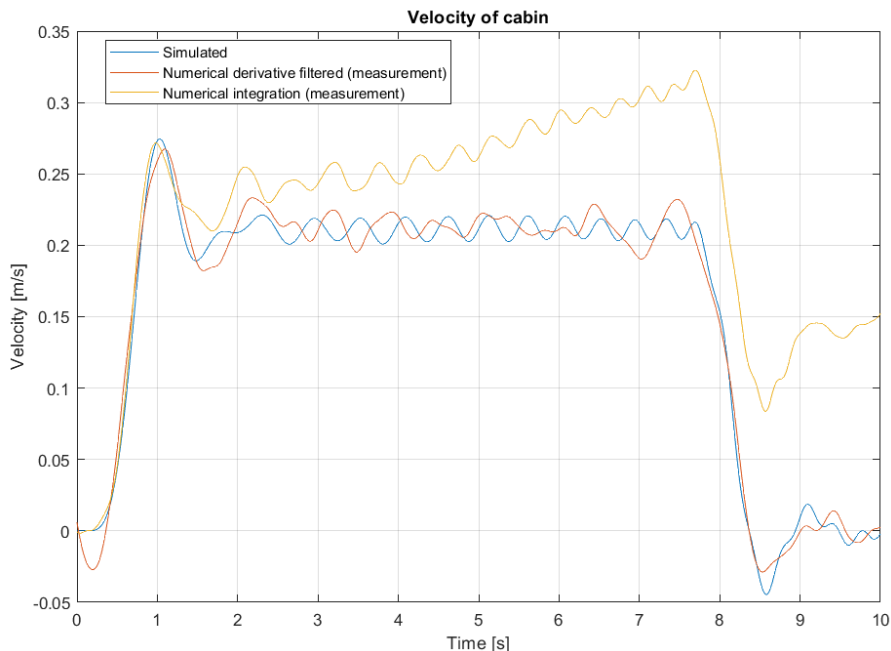


Figure 1.7: Velocity of cabin for simulated results and from measured data

When validating the behavior of the simulated model it is interesting to compare the simulation results on the cabin side with the counterweight side. Fig. 1.8 show the deflection and deformation velocity of the rope on each side of the drive sheave. During the simulated elevator ride, the cabin moves up and the counterweight moves down. The stiffness of the rope increases when the length decreases as shown in the stiffness matrix K in Eq. (1.5). In Fig. 1.8 the ropes deflect as expected. The initial deflection on the cabin side is high, peaks around the point of maximum acceleration, and decreases with a constant slope when the length decreases, and the acceleration oscillates around a constant value.

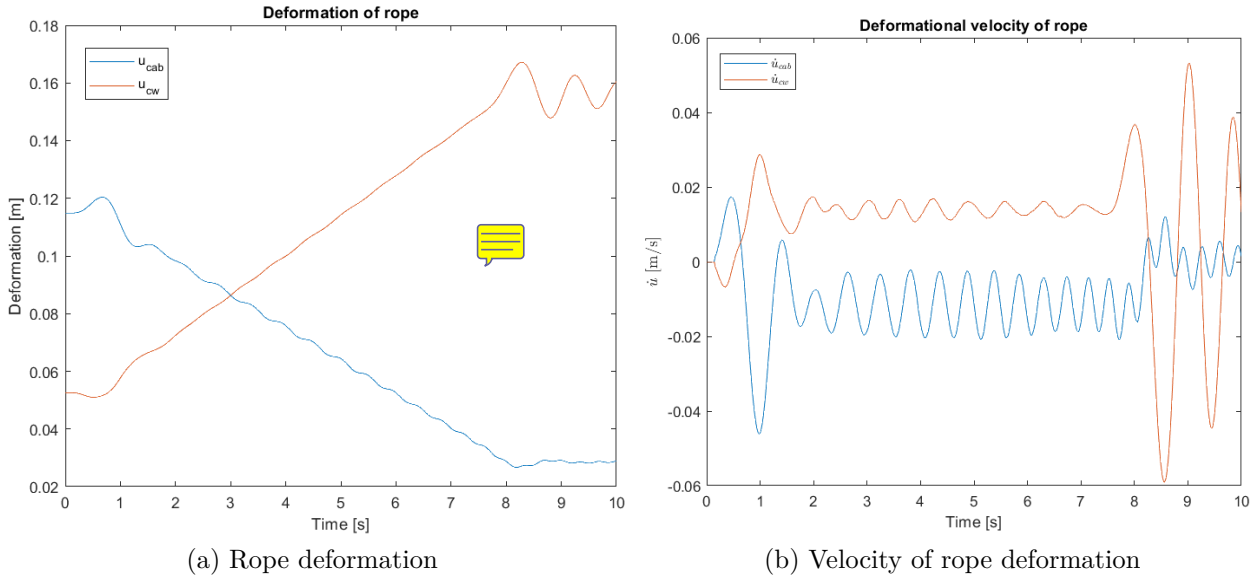


Figure 1.8: Simulated deformation of rope and deformation velocity of rope in time domain on both cabin/counterweight sides.

Fig. 1.8 shows that the deformation velocity of the rope on the cabin side is highest around the points of maximum acceleration and deceleration. The amplitude of the rope vibration peaks during acceleration. This makes sense because the damping coefficient c is modeled as being linearly proportional with the rope stiffness K as shown in Eq. (1.12). The rope on the counterweight side behaves exactly the opposite.

1.6 Conclusion

In this project, the dynamics of an elevator-system are investigated using a numerical model to simulate an elevator ride. Results from the simulation show that the model behaves in accordance with specified virtual experiment data. As it was not possible to conduct the elevator experiment, the discrete model developed in this project should be considered purely theoretical. The virtual data suggests that the simulation behaves as expected, but this is no guarantee that results will match the uncertainties and sources of error from an actual experiment. If the experiment was performed, parameters such as the effective drive sheave radius should be determined experimentally to dial in the model.

A | Rope experiment

Purpose

The purpose of the experiment is to determine the stiffness per unit length, EA , and the viscous damping coefficient, c , for the elastic rope used in the elevator system.

List of equipment and experimental setup

The experiment is performed using the following equipment:

- A piece of the rope.
- 1 bucket.
- 1 accelerometer.
- 1 yard stick.
- A GP-61K scale.
- Various objects of different mass (3 safety shoes, 1 screwdriver and 1 french wrench).



Figure A.1: Test setup.

The same setup is used for measuring the static deflection and for determining the damping of the rope. One end of the rope is tied to a bucket and the other is fastened to a metal rail in order to let the bucket swing freely. This is seen on Fig. A.1.

For the static deflection experiment, the bucket is either empty or containing various items to vary the force pulling on the rope.

For the damping experiment, the accelerometer is placed in the middle of the bucket. The accelerometer is placed so the positive z-axis is pointing upwards.

Experiment procedure

The experiment is split into two parts, with two different procedures:

Experiment for determining the stiffness of the rope:

The static deflection of the rope under influence of different weights is measured. Before the start of the experiment, an undeflected length of 20 cm on the rope is marked up. The rope is tied to the bucket and the deformed length of the control length of rope is measured. This is repeated with various items with different weights in the bucket. Each measurement happens

when the rope with the bucket is static.

Experiment for determining the damping of the rope:

The acceleration of a mass at the end of the rope is measured. The mass used is the same bucket as is used in the static deflection. The accelerometer is placed at the bottom of the bucket and connected to the PC. The bucket is pulled straight downwards to initiate oscillation of the system. The bucket is let go so that it can oscillate freely until it reaches equilibrium.

Test results: Static deflection

Table A.1 shows the results from the static deflection experiment.

Exp. no.	Mass of weight [g]	Length of control piece of rope [mm]
Ctr.	0	200
1	701	250
2	757	260
3	994	285
4	1417	320
5	2128	352
6	2844	365

Table A.1: Test data from static deflection test

The mass and the free length of the rope is measured.

$$l_0 = 700 \text{ mm} \text{ and } m_{700\text{mm}} = 19.6 \text{ g}$$

Test results: Damping coefficient

The test results from the damping coefficient experiment consist of 316 coupled measurements of time and acceleration of the bucket.

Data processing - static deflection

The deflected lengths are measured with respect to a control length of 20 cm. In order to calculate the stiffness, EA, the weight of that control length is needed. The weight of the rope pr. unit length is calculated in Eq. (A.1) and used to determine the weight of the control length.

$$m_{200\text{mm}} = \frac{m_{700\text{mm}}}{l_0} \cdot 200 \text{ mm} = 5.6 \text{ g} \quad (\text{A.1})$$

The stiffness per unit length is determined from Eq. (A.2), that is set up from force equilibrium.

$$\sum F_z = 0 : m \cdot g - k \cdot x = 0$$

$$EA = \frac{m \cdot g \cdot L}{x} \quad (\text{A.2})$$

Exp. no.	1	2	3	4	5	6	Average
Stiffness, EA [N]	27.7	25.0	23.1	23.3	27.5	33.9	26.7

Table A.2: Determined stiffness for each experiment and the calculated average

The relationship between the elongation and the force pulling on the rope is shown on Fig. A.2 (a).

Data processing - damping coefficient

The test results are low-pass filtered using a 2. order Butterworth filter. The peaks of the acceleration are located and used to determine the damping coefficient according to the logarithmic decrement method. An exponential function is fitted on the peaks of the oscillating accelerations. The function is expressed in Eq. (A.3).

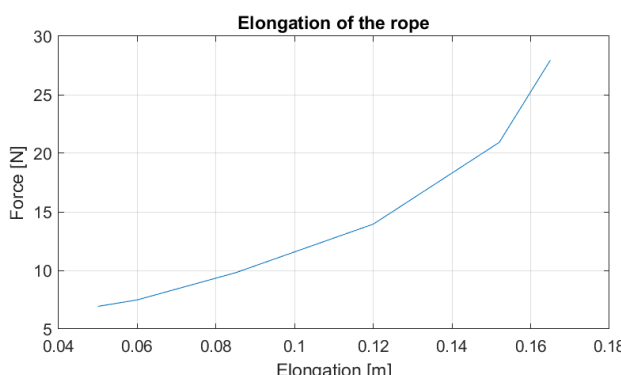
$$\boxed{14.16 \cdot e^{-0.345 \cdot t}} \quad (\text{A.3})$$

Fig. A.2 (b) shows the exponential function fitted to the peaks of the acceleration.

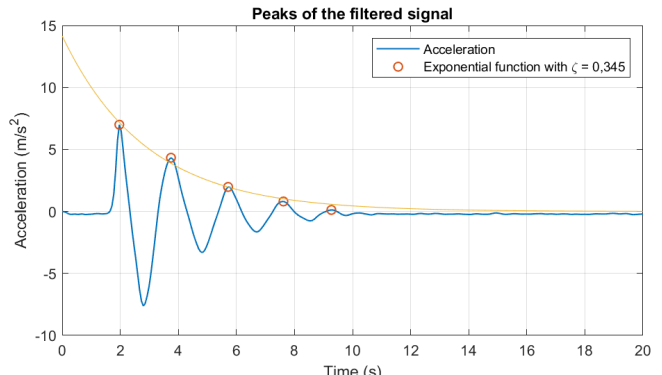
This yields a damping ratio of $\zeta = 0,345$. The damping coefficient is calculated using the mass of the bucket and the mean k-value for the rope, see Eq. (A.4).

$$c = \zeta \cdot c_{cr} \text{ and } c_{cr} = 2 \cdot \sqrt{k \cdot m} \quad (\text{A.4})$$

The damping coefficient is determined to be $c = 6.68 \frac{\text{N} \cdot \text{s}}{\text{m}}$.



(a) Data from stiffness experiment



(b) Data from damping experiment

Figure A.2: Resulting plots from data processing of the experiments.

Discussion

There are several uncertainties regarding the experiment to determine the stiffness of the rope. The control length of the rope is marked up using a ruler and a permanent marker. When the rope is stretched, the lines marking the start and end of the control length are also stretched out. This reduces the accuracy with which the elongation is measured.

The stiffness is determined based off of 6 datapoints, which is quite a small test pool. More datapoints would have given a more adequate representation of the stiffness of the rope. The stiffness is taken as a mean value of the datapoints, including the points in the nonlinear area.

For the experiment determining the damping coefficient, the maximum amount of peaks achieved is five. This makes sense as the rope has very high damping, however more oscillations might have yielded a more accurate ζ -value. However, the exponents are determined with 95 % confidence bounds. Furthermore, the bucket which holds the accelerometer is not confined to movement in only one axis, but it can swing freely around all three axes. Ideally, it should only accelerate in one direction. As stated in the procedure, it is attempted to start the oscillation of the bucket by pulling the bucket straight down. This is not very precise.

Conclusion

The stiffness of the rope, EA, is found to be $EA = 26.7 \text{ N}$. The damping coefficient of the rope is found to be $c = 6.68 \frac{\text{N} \cdot \text{s}}{\text{m}}$.